Microchimica Acta (2018) 185: 502
https://doi.org/10.1007/s00604-018-3028-7

ORIGINAL PAPER

# Ultrasensitive determination of thrombin by using an electrode modified with $WSe_2$ and gold nanoparticles, aptamer-thrombin-aptamer sandwiching, redox cycling, and signal enhancement by alkaline phosphatase

Yi-Han Wang[1] · Huan Xia[1] · Ke-Jing Huang[1] · Xu Wu[2] · Ying-Ying Ma[1] · Rui Deng[1] · Yun-Fei Lu[1] · Zi-Wei Han[1]

Received: 24 July 2018 / Accepted: 26 September 2018 / Published online: 9 October 2018


## Abstract

A sensitive aptamer/protein binding-triggered sandwich assay for thrombin is described. It is based on electrochemical-chemical-chemical redox cycling using a glassy carbon electrode (GCE) that was modified with $WSe_2$ and gold nanoparticles (AuNPs). The AuNPs are linked to thrombin aptamer 1 via Au-S bonds. Thrombin is first captured by aptamer 1 and then sandwiched through the simultaneous interaction with AuNPs modified with thrombin-specific aptamer 2 and signalling probe. Subsequently, the DNA-linked AuNP hybrids result in the capture of streptavidin-conjugated alkaline phosphatase onto the modified GCE through the specific affinity reaction for further signal enhancement. As a result, a linear range of 0–1 ng $mL^{-1}$ and a detection limit as low as 190 fg $mL^{-1}$ are accomplished. The specificity for thrombin is excellent. Conceivably, this strategy can be easily expanded to other proteins by using the appropriate aptamer.

**Keywords** Tungsten diselenide nanosheets · Electrochemical biosensor · Sandwiched structure · Protein · Signal enhancement

## Introduction

The recognition of thrombin (TB) is usually achieved by using antibodies. However, aptamers are more easily synthesized and modified. Aptamers based strategy have the advantages of long-term storage, inexpensive and high stability [1]. Two kinds of aptamers with specific binding affinity to TB are obtained by SELEX technique. One is a 15-mer called thrombin aptamer 1 (TBA1) which was first reported by Bock et al. [2]. The TBA1 binds to the fibrinogen-binding site of TB. The other is a 29-mer called thrombin aptamer 2 (TBA2) which interacts with the heparin-binding site of TB. The two aptamers do not interfere with each other's binding. In this case, TB-sensing methods have been constructed by aptamer-target-aptamer sandwiched structure, such as electrochemical biosensors [3–5], electrochemiluminescence biosensors [6, 7], fluorometric biosensors [8], and colorimetric biosensors [9]. Among them, electrochemical biosensors have many intrinsic advantages such as rapid response, relatively low cost and high sensitivity. In addition, the sensitivity of the sensor is closely related to nanomaterials. Transition-metal dichalcogenides (TMDCs), as graphene-like 2D layered materials, have significant merits such as superior conductivity, excellent chemical stability and large surface area. Among them, the tungsten selenide ($WSe_2$) has become an advanced materials in electrochemical sensors [10, 11]. Metal nanoparticles, especially gold nanoparticles (AuNPs) are widely used as signal amplifiers to improve the sensitivity of assays due to their good biocompatibility, large surface area and can accelerating the electron transfer [12, 13].

In this study, a sensitive electrochemical aptamer-target-aptamer sandwiched biosensor for the detection of protein is fabricated by using TB as an experimental model based on electrochemical-chemical-chemical (ECC) redox cycling and enzyme signal enhancement strategy. The principle of the biosensor is demonstrated in Scheme 1. $WSe_2$ nanosheets with

**Electronic supplementary material** The online version of this article (https://doi.org/10.1007/s00604-018-3028-7) contains supplementary material, which is available to authorized users.

✉ Ke-Jing Huang
kejinghuang@163.com

[1] College of Chemistry and Chemical Engineering, Xinyang Normal University, Xinyang 464000, China

[2] School of Physics and Electronic Engineering, Xinyang Normal University, Xinyang 464000, China

superior conductivity and large specific area are used as a good substrate for sensing. It is well known that, AuNPs can form links with aptamers through Au-S or Au-NH chemical bonds [13, 14]. This sensor combined the merits of $WSe_2$ with those of AuNPs to immobilize large amount of thiol-terminated TBA1. Moreover, MCH used as blockers to inactivate the modified electrode surface and reduce non-specific adsorption, which maintained correct direction of DNA on the electrode interface. Then, the TBA1/AuNPs/$WSe_2$ modified electrode capture thrombin as a target. AuNPs can serve as a "carrier" to provide more active sites for the immobilization of TBA2 and biotinylated signal probe. Thrombin initiated the formation of aptamer-target-aptamer sandwiched structure as DNA-linked AuNP hybrids. Subsequently, amounts of streptavidin-conjugated alkaline phosphatase (SA-ALP) are immobilized on the modified electrode surface through the specific affinity reaction between streptavidin (SA) and biotin for further signal enhancement. The alkaline phosphatase (ALP) can effectively hydrolyze the ascorbic acid 2-phosphate (AAP) to produce ascorbic acid (AA), thus triggering ECC redox cycling to amplify electrochemical signal. Due to the multiple signal enhancement of $WSe_2$, AuNPs, enzyme, ECC redox cycling and aptamer-target-aptamer sandwiched structure, high sensitivity for TB detection is realized.

## Experimental section

### Materials and reagents

Analytical grade chemicals (Se, $Na_2WO_4{\cdot}2H_2O$, $NaBH_4$, $HAuCl_4{\cdot}4H_2O$, $Na_3C_6H_5O_7{\cdot}2H_2O$, NaCl, DMF, KCl, $MgCl_2$, $CaCl_2$, $K_2HPO_4$, $KH_2PO_4$, $K_3Fe[CN]_6$, $K_4Fe[CN]_6$) were obtained from Aladdin Chemicals Co., Ltd. (Shanghai, China, www.aladdin-e.com). 6-Mercapto-1-hexanol (MCH), tris-(hydroxymethyl) aminomethane hydrochloride (Tris-HCl), immunoglobin G (IgG), hemoglobin (HB), prostate-specific antigen (PSA), tris-(2-carboxyethyl) phosphine hydrochloride (TCEP), AAP, FcM, SA-ALP and TB were purchased from Sigma-Aldrich (Saint Louis, MO, USA, www.sigmaaldrich.com). All oligonucleotides (purified by high-performance liquid chromatography) were synthesized by Sangon Biotechnology Co., Ltd. (Shanghai, China, www.sangon.com). The TBA2 sequence was prepared according to reference [15]. The sequences were listed in Table S1.

### Apparatus

An EC550 electrochemical workstation (Wuhan, Gaoss Union, China, www.gaossunion.com) was used to carry out cyclic voltammetric (CV), electrochemical deposition, electrochemical impedance spectroscopy (EIS), chronocoulometry (CC) and differential pulse voltammetry (DPV) with three-electrode system including a modified glassy carbon electrode (GCE, $\Phi = 3$ mm), $Hg/Hg_2Cl_2$ reference electrode and platinum auxiliary electrode. S-4800 scanning electron microscope (SEM, Hitachi Co, Japan, www.hitachi.com), a JEM 2100 transmission electron microscope (TEM, JEOL, Tokyo, Japan, www.jeol.de/electronoptics-en/index.php) and a K-ALPHA 0.5EV X-ray Photoelectron Spectrometer (XPS, Thermo Fisher Scientific, UK, www.thermofisher.com) were used for characterizing various samples.

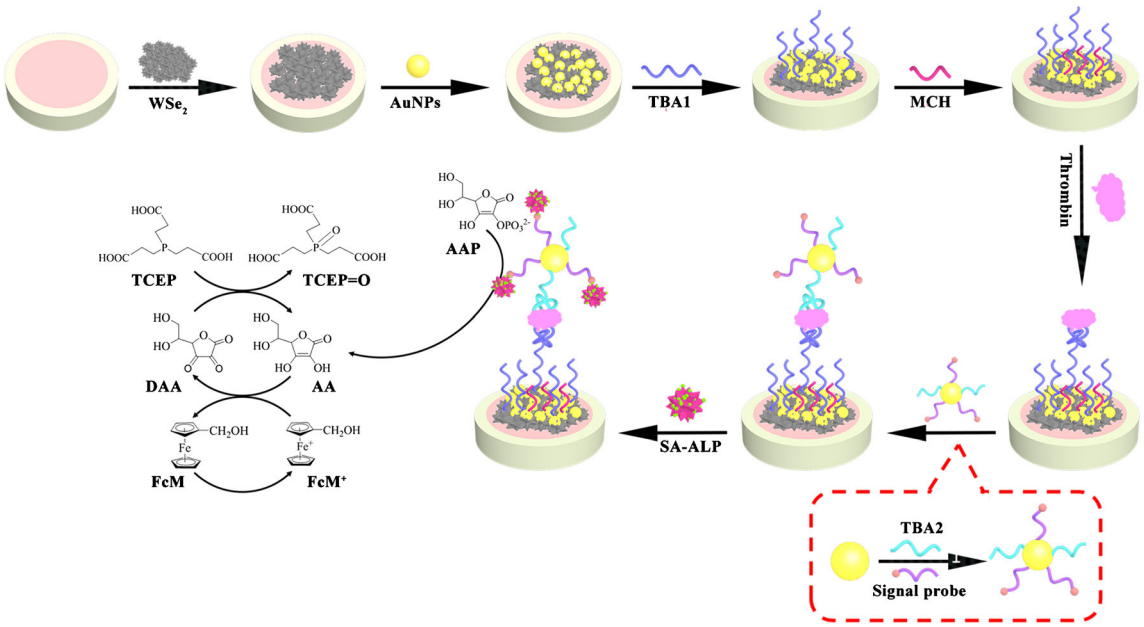


**Scheme 1** Fabrication process of the assay for TB detection

## Assembly of the modified electrodes

Preparation of the TBA2 and signal probe modified AuNPs hybrids were as follows: TBA1, TBA2 and biotinylated signal probe were dissolved in 100 mM Tris-HCl solution (pH 7.0, 50 mM NaCl, 20 mM KCl and 10 mM $MgCl_2$) containing 100 times of TCEP in order to reduce disulfide bonds. First, 1 mL AuNPs, 20 μL 0.1 mM of TBA2 and signal probe were mixed in centrifuge tube and incubated at 4 °C for 16 h to obtain the DNA-linked AuNPs composite. The unconjugated TBA2 and signal probe were eliminated after centrifugation and washed with phosphate buffer (pH 7.0). Finally, the DNA-linked AuNPs composites were dispersed in 1 mL phosphate buffer for further use.

The bare GCE electrode was pretreated with 0.05 μm alumina powders. Then, 8 μL 1 mg $mL^{-1}$ of $WSe_2$ was applied onto electrode to form a good disseminated film. After washed with phosphate buffer, the $WSe_2$/GCE was immersed into 0.1% $HAuCl_4$ solution to deposit AuNPs at −0.2 V and the deposition time was 25 s. After coating 8 μL 2 μM of TBA1 on the surface of AuNPs/$WSe_2$/GCE and kept at room temperature for 12 h, the electrode was immersed 6 μL 1 mM of MCH for 40 min. Then, the electrode was washed with phosphate buffer (pH 7.0). TB was dissolved in TE buffer (20 mM Tris-HCl, 140 mM NaCl, 5 mM KCl, 5 mM $MgCl_2$ and 1 mM $CaCl_2$, pH 7.4). After that, 8 μL TB solutions with different concentration were dropped onto the MCH/TBA1/AuNPs/$WSe_2$/GCE surface and incubated at 37 °Cfor 70 min. Subsequently, 10 μL of the DNA-linked AuNPs hybrids was dropped on electrode and kept for 90 min to obtain a aptamer-target-aptamer sandwiched structure. The modified electrode then reacted with 10 μL 0.1 mg $mL^{-1}$ of SA-ALP for 1 h. Lastly, the electrode was incubated in 10 mM Tris buffer (1 mM $MgCl_2$, pH 8.0) with 5 mM AAP for 30 min.

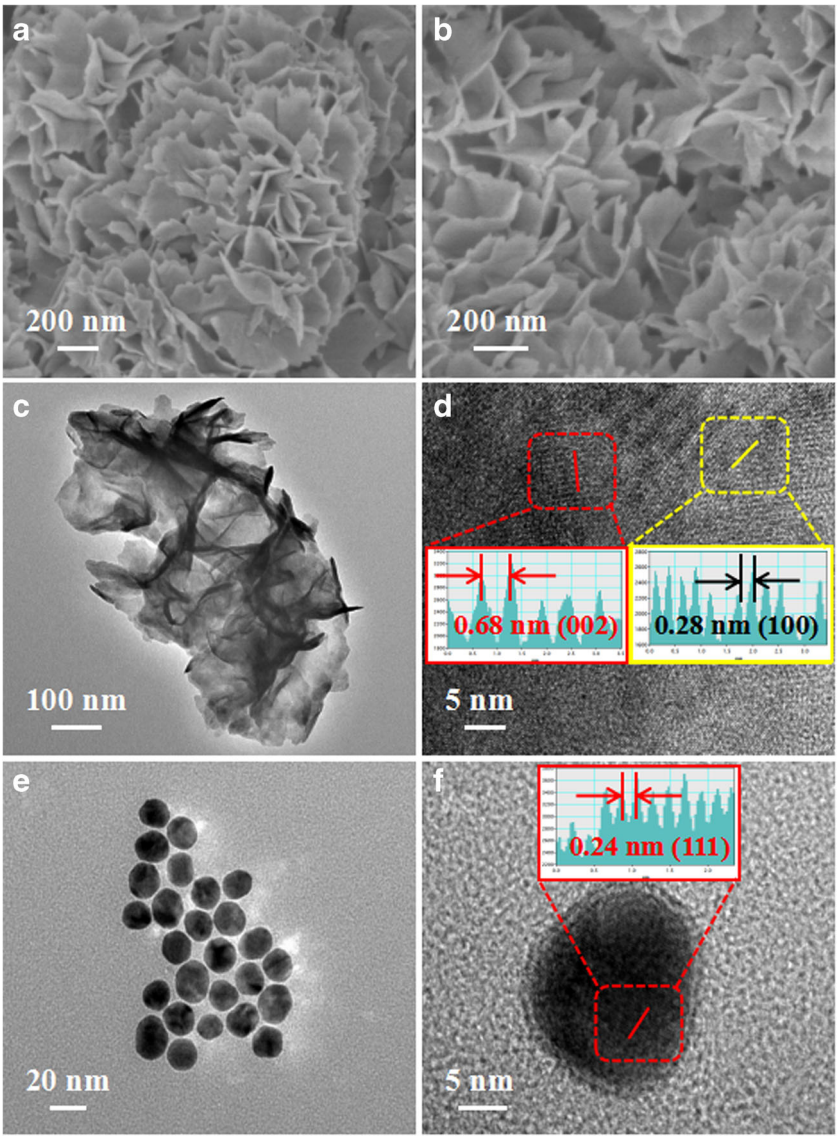


**Fig. 1** SEM (**a**, **b**), TEM (**c**) and HRTEM (**d**) images of $WSe_2$. TEM (**e**) and HRTEM (**f**) images of AuNPs; the inset of (**d** and **f**) show the measurement of lattice interfaces

## Experimental measurements

CV was performed in 0.1 M phosphate buffer (pH 7.0) containing 10 mM $[Fe(CN)_6]^{3-/4-}$ and 0.1 M KCl, scanning from −0.2 V to 0.6 V at a scan rate of 100 $mVs^{-1}$. EIS was carried out in phosphate buffer (pH 7.0) containing 10 mM $[Fe(CN)_6]^{3-/4-}$ and 0.1 M KCl in the frequencies swept from 0.1 Hz to 100 kHz with 5 mV as the amplitude at a potential of 0.2 V. DPV measurements were taken in Tris buffer (5 mM TCEP, 2 mM FcM) with the pulse amplitude of 0.005 V, pulse width of 0.05 s and the pulse period of 0.2 s. Each measurement was repeated three times.

## Results and discussion

### Choice of materials

Nanomaterials with many specific properties have been widely used in the field of electrochemical analysis. Two-dimensional transition metal dichalcogenides, such as $MoS_2$ and $WS_2$, have been used in electrochemical biosensor due to their large specific surface areas and chemical stability [16, 17]. However, the electrical conductivity of $MoS_2$ or $WS_2$ is not that good, which limits their application. As a key member of two-dimensional transition metal dichalcogenides, $WSe_2$ with a structure composed of three stacked atom layers (Se-W-Se) bonded together by van der Waals forces has been explored as a promising material for various fields, such as hydrogen evolution, photocatalysts and electrochemical sensing [18–21]. Importantly, compared to $WS_2$, $WSe_2$ has higher intrinsic electrical conductivity due to the more metallic nature of Se. Furthermore, the unsaturated Se-edges in $WSe_2$ are electro-catalytically active and beneficial for the electrochemical sensing [16]. In this work, $WSe_2$ nanosheets was applied as the substrate platform to fabricate assay for the sensitive detection of TB.

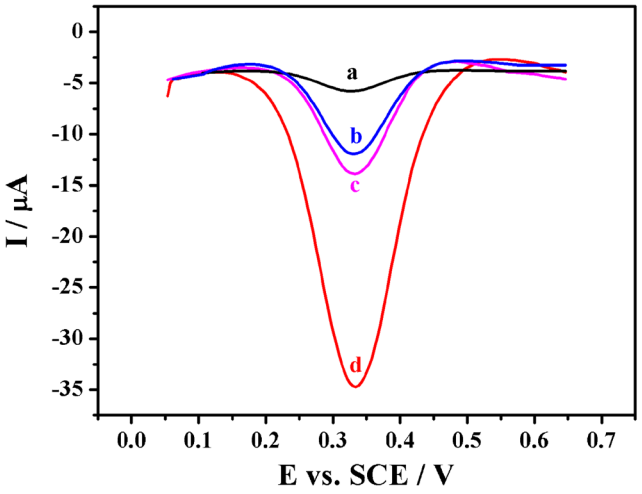


**Fig. 3** DPV curves of different electrodes: without DNA-linked AuNPs composite (a), without SA-ALP (b), without TB (c), SA-ALP/DNA-linked AuNPs/TB/MCH/TBA1/AuNPs/$WSe_2$/GCE (d)

### Morphological and structural characterizations

SEM was used to identify the morphologies of the product. From Fig. 1a, b, it can be expressly observed that the $WSe_2$ has many ultra-thin sheets tending to different directions to form hierarchical structure with large surface area and porous channels. This structure facilitates the construction of sensors [22]. The TEM of $WSe_2$ in Fig. 1c coincides with the above SEM. Figure 1d shows the high-resolution TEM (HR-TEM) image of the $WSe_2$ with more crystal structure information. The lattice spacings of approximately 0.68 nm and 0.28 nm which correspond to the D-spacing of the (002) and (100) lattice fringe of $WSe_2$. The result is in good agreement with XRD pattern. Figure 1e shows the average size of AuNPs is about 20 nm. The HR-TEM in Fig. 1f exhibits an interplanar spacing of 0.24 nm, which is well unanimous with the (111) plane of AuNPs. The insets of Fig. 1d, f show the measure of lattice interfaces. Furthermore, the size distribution of AuNPs

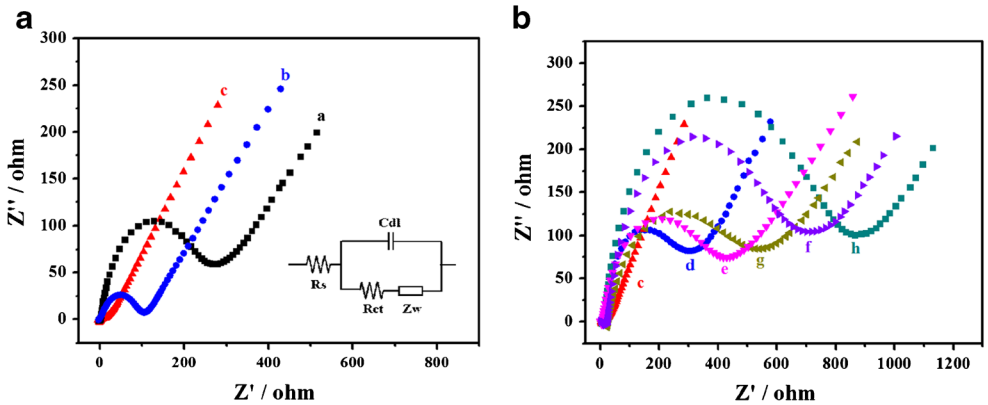


**Fig. 2** EIS (**a**, **b**) of different electrodes in phosphate buffer (pH 7.0) containing 10 mM $[Fe(CN)_6]^{3-/4-}$ and 0.1 M KCl: GCE (a); $WSe_2$/GCE (b); AuNPs/$WSe_2$/GCE (c); TBA1/AuNPs/$WSe_2$/GCE (d); MCH/TBA1/AuNPs/$WSe_2$/GCE (e); TB/MCH/TBA1/AuNPs/$WSe_2$/GCE (f); DNA-linked AuNPs/TB/MCH/TBA1/AuNPs/$WSe_2$/GCE (g); SA-ALP/DNA-linked AuNPs/TB/MCH/TBA1/AuNPs/$WSe_2$/GCE (h)

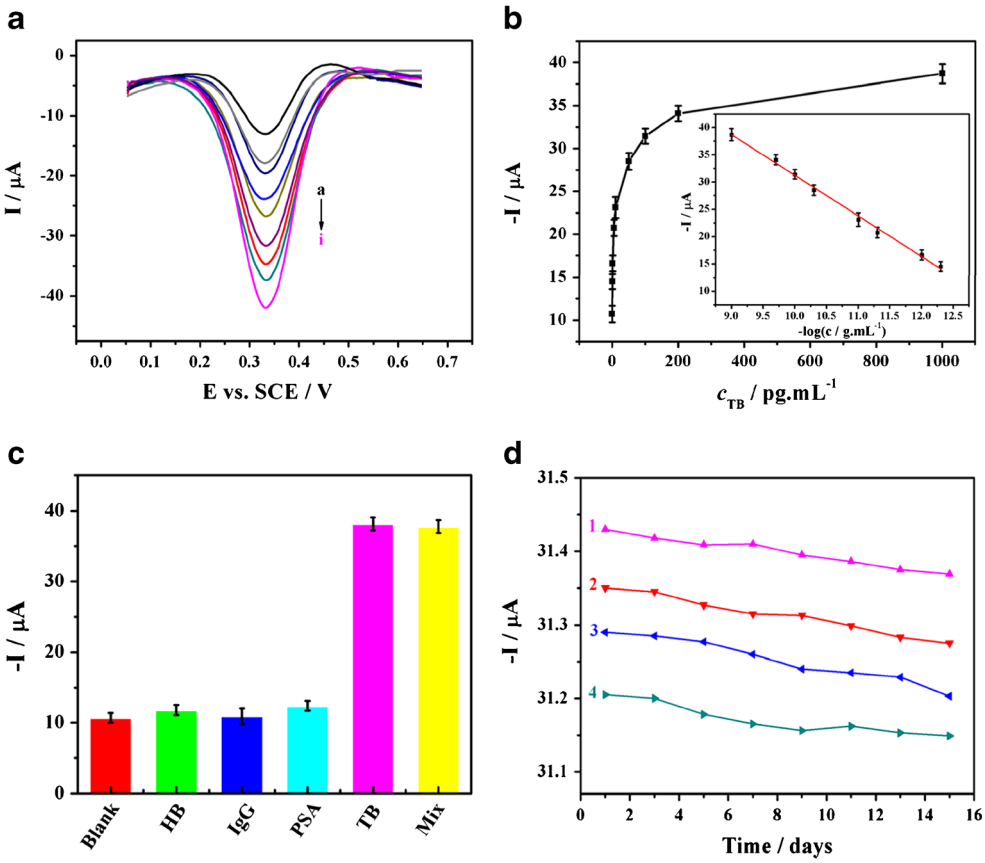


**Fig. 4** **a** DPV of different concentrations of TB in Tris buffer (a-i: 0, 0.5, 1, 5, 10, 50, 100, 200, 1000 pg mL$^{-1}$). **b** The curve of DPV values versus TB concentration, inset shows the calibration plot. **c** Detection of various solution in Tris buffer. **d** Signal intensities of the four modified electrodes within 15 days

and DNA-linked AuNPs composites are further investigated by dynamic light scattering (DLS) in Fig. S1. The average dynamic size of DNA-linked AuNPs composites (34.5 nm, Fig. S1b) is obviously greater than that of AuNPs (21.7 nm, Fig. S1a), proving that the successful assembly of DNA-linked AuNPs composites. The measured particle size is slightly larger than the actual size due to the dust in air [23]. X-ray powder diffractometer, Raman spectra, SEM-energy dispersive X-ray and X-ray photoelectron spectroscopy (XPS) of the $WSe_2$ are shown in Fig. 2S.

## Electrochemical characterization of electrodes

EIS is effective means for probing the electrochemical properties of electrode surfaces. Figures 2a, b display the EIS at different modification steps. In the inset of Fig. 2a, Randles's equivalent circuit is used in EIS for explanation of spectra [24]. The charge transfer resistance ($R_{ct}$) is the important parameter. Comparing with the bare GCE (curve a), the $R_{ct}$ significantly decreases after the electrode modified with $WSe_2$ (curve b) and AuNPs (curve c). However, the $R_{ct}$ increases in turn after the electrode incubating negatively charged TBA1 (curve d) and MCH (curve e). The $R_{ct}$ value keeps increasing after the electrode surface is treated with biological macromolecule TB (curve f), which is ascribed to the effect of steric hindrance. After the modified electrode is incubated with DNA-linked AuNPs composite (curve g), the diameter of semicircle decreases. Furthermore, a further increase of $R_{ct}$ value is obtained when the electrode is incubated with SA-ALP (curve h). CV results was in agree with that of the EIS (Fig. S3).

## Optimization

The following parameters were optimized: (a) TBA1 loading; (b) incubation time of TB; (c) incubation time of DNA-linked AuNP composite; Respective data and Figures are given in the

**Table 1** Different strategies for TB detection

| Detection method | Linear range (pM) | LOD (pM) | References |
|---|---|---|---|
| Electrochemical aptasensor | 0.3–54 | 0.14 | [25] |
| Electrochemical aptasensor | 100–25,000 | 20 | [26] |
| Electrochemiluminescence | 10–10,000 | 6.3 | [6] |
| Electrochemical aptasensor | 10–50,000 | 5.6 | [27] |
| Electrochemiluminescence | 0.4–1000 | 0.23 | [7] |
| Fluorescence | 0.25–25,000 | 8.9 | [28] |
| Fluorescence | 10,000–80,000 | 1300 | [29] |
| Fluorescence | 50–100,000 | 15 | [30] |
| Electrochemical aptasensor | 0.014–28 | 0.0053 | This work |

Electronic Supporting Material (Fig. S4). The following experimental conditions were found to give best results: (a) optimal loading: 2 μM; (b) optimal incubation time: 70 min; (c) optimal incubation time: 90 min.

In order to investigate the feasibility of this sensor, different modified electrodes were detected. As shown in Fig. 3, in the absence of SA-ALP (curve a) or DNA-linked AuNPs composites (curve b), no obvious signal is observed at the modified electrodes. The DPV peak currents is very small at the electrode without TB (curve c) due to sandwiched structure can not be formed. However, a clearly signal is obtained at the modified electrode in the presence of all substances (curve d).

### Analytical performance

To illustrate the applicability of the designed method, a series of concentrations of TB are detected under the optimal conditions. Figure 4a, b display the DPV peaks increases with the increase of TB concentration varying from 0 pg $mL^{-1}$ to 1 ng $mL^{-1}$ and the inset of Fig. 4b depicts linear relationship. The linear equation is expressed as $I(\mu A) = -7.46 \log(c/g\ mL^{-1}) - 105.80$ ($R = 0.995$), and the detection limit (LOD) is detected as $1.9 \times 10^{-13}$ g $mL^{-1}$ ($S/N = 3$). As shown in Table 1, the analytical performance of the method is compared with other assays for the detection of TB [6, 7, 25–30]. To explore the selectivity and specificity of the sensor, interfering agents including HB (0.2 g $mL^{-1}$), IgG (20 ng mL-1) and PSA (2 ng $mL^{-1}$) were examined under the same constraints. Figure 4c shows these interferences have negligible effect on the peak current compared with the blank sample. It is obvious that the DPV peak current is almost the same as that of the TB when HB, IgG and PSA (0.2 g $mL^{-1}$, 20 ng $mL^{-1}$, 2 ng $mL^{-1}$, respectively) are mixed with TB (1 ng $mL^{-1}$). The reproducibility was monitored by DPV measurements for five electrodes under the same constraints, and the relative standard deviation (RSD) of 4.2% was obtained. Furthermore, the stability of the strategy was examined by using four electrodes that prepared independently. As shown in Fig. 4d, the DPV peak currents have no obvious change after the electrodes were kept at 4 °C over 2 weeks (one test per 2 days), suggesting excellent stability.

### Real sample analysis

To assess the application of the assay, recovery experiments were performed. Human serum samples were obtained from the affiliated hospital of Xinyang Normal University (Xinyang, China). The serum sample was extracted by centrifugation at 1680 rcf three times. Then 1 mL serum sample was added into 10 mL phosphate buffer. 0.5 mL TB with different concentrations was added into 10 mL diluted serum sample. Then the sample was detected with the assay. The results are listed in Table S2. The recoveries are 91.1%–108.2% and RSDs are 3.8%–6.5%. The same samples were also detected by ELISA method. As shown in Table S2, the results display a good agreement between two assays.

## Conclusion

In conclusion, a sensitive sandwich method for TB detection was fabricated based on ECC redox cycling and enzyme signal enhancement strategy. The method displayed following attractive features. Firstly, the $WSe_2$ nanosheets with high surface area were applied as nano-carriers leading to the deposition of more AuNPs on the materials surface. Secondly, AuNPs with good biocompatibility could provide more sites for immobilization larger amounts of aptamers. Subsequently, the DNA-linked AuNPs composites resulted in the capture of many SA-ALPs onto the electrode interface to amply the signal. Thirdly, ECC redox cycling and sandwiched structure could further magnify signal respond. However, it should be noted that this method suffered a major limitation: it required more time to prepare nanomaterials and modified electrode, which also needed skilled people.

**Acknowledgments** This work was supported by the National Natural Science Foundation of China (21475115), Henan Provincial Science and technology innovation team (C20150026), Nanhu Scholars Program of XYNU and Henan Science and Technology Cooperation Project (172106000064).

**Compliance with ethical standards** The author(s) declare that they have no competing interests.

## References

1. Tan Z, Feagin TA, Heemstra JM (2016) Temporal control of aptamer biosensors using covalent self-caging to shift equilibrium. J Am Chem Soc 138(20):6328–6331. https://doi.org/10.1021/jacs.6b00934
2. Bock LC, Griffin LC, Latham JA, Vermaas EH, Toole JJ (1992) Selection of single-stranded DNA molecules that bind and inhibit human thrombin. Nature 355(6360):564–566. https://doi.org/10.1038/355564a0
3. Zhang Y, Xia J, Zhang F, Wang Z, Liu Q (2018) Ultrasensitive label-free homogeneous electrochemical aptasensor based on sandwich structure for thrombin detection. Sensors Actuators B Chem 267:412–418. https://doi.org/10.1016/j.snb.2018.04.053
4. Yang Y, Yang Z, Lv J, Yuan R, Chai Y (2017) Thrombin aptasensor enabled by Pt nanoparticles-functionalized co-based metal organic frameworks assisted electrochemical signal amplification. Talanta 169:44–49. https://doi.org/10.1016/j.talanta.2017.03.037
5. He B (2018) Sandwich electrochemical thrombin assay using a glassy carbon electrode modified with nitrogen-and sulfur-doped graphene oxide and gold nanoparticles. Microchim Acta 185(7):344. https://doi.org/10.1007/s00604-018-2872-9
6. Li Y, Li Y, Xu N, Pan J, Chen T, Chen Y, Gao W (2017) Dual-signal amplification strategy for electrochemiluminescence sandwich

biosensor for detection of thrombin. Sensors Actuators B Chem 240:742–748. https://doi.org/10.1016/j.snb.2016.09.043
7. Wang X, Sun D, Tong Y, Zhong Y, Chen Z (2017) A voltammetric aptamer-based thrombin biosensor exploiting signal amplification via synergetic catalysis by DNAzyme and enzyme decorated AuPd nanoparticles on a poly (o-phenylenediamine) support. Microchim Acta 184(6):1791–1799. https://doi.org/10.1007/s0060
8. Zhao X, Li S, Xu L, Ma W, Wu X, Kuang H, Xu C (2015) Up-conversion fluorescence "off-on" switch based on heterogeneous core-satellite assembly for thrombin detection. Biosens Bioelectron 70:372–375. https://doi.org/10.1016/j.bios.2015.03.068
9. Liang G, Cai S, Zhang P, Peng Y, Chen H, Zhang S, Kong J (2011) Magnetic relaxation switch and colorimetric detection of thrombin using aptamer-functionalized gold-coated iron oxide nanoparticles. Anal Chim Acta 689(2):243–249. https://doi.org/10.1016/j.aca.2011.01.046
10. Chen YX, Zhang WJ, Huang KJ, Zheng M, Mao YC (2017) An electrochemical microRNA sensing platform based on tungsten diselenide nanosheets and competitive RNA-RNA hybridization. Analyst 142(24):4843–4851. https://doi.org/10.1039/c7an01244f
11. Karfa P, Madhuri R, Sharma PK (2017) Multifunctional fluorescent chalcogenide hybrid nanodots ($MoSe_2$: CdS and $WSe_2$: CdS) as electro catalyst (for oxygen reduction/oxygen evolution reactions) and sensing probe for lead. J Mater Chem A 5(4):1495–1508. https://doi.org/10.1039/C6TA08172J
12. Xu Q, Wang G, Zhang M, Xu G, Lin J, Luo X (2018) Aptamer based label free thrombin assay based on the use of silver nanoparticles incorporated into self-polymerized dopamine. Microchim Acta 185(5):253. https://doi.org/10.1007/s00604-018-2787-5
13. Shuai HL, Huang KJ, Xing LL, Chen YX (2016) Ultrasensitive electrochemical sensing platform for microRNA based on tungsten oxide-graphene composites coupling with catalyzed hairpin assembly target recycling and enzyme signal amplification. Biosens Bioelectron 86:337–345. https://doi.org/10.1016/j.bios.2016.06.057
14. Zhang H, Guo Z, Dong H, Chen H, Cai C (2017) An electrochemiluminescence assay for sensitive detection of methyltransferase activity in different cancer cells by hybridization chain reaction coupled with a G-quadruplex/hemin DNAzyme biosensing strategy. Analyst 142(11):2013–2019. https://doi.org/10.1039/C7AN00486A
15. Wang W, Xu DD, Pang DW, Tang HW (2017) Fluorescent sensing of thrombin using a magnetic nano-platform with aptamer-target-aptamer sandwich and fluorescent silica nanoprobe. J Lumin 187:9–13. https://doi.org/10.1016/j.jlumin.2017.02.059
16. Wang XQ, Chen YF, Qi F, Zheng BJ, He JR, Li Q, Li PJ, Zhang WL, Li YR (2016) Interwoven WSe 2 /CNTs hybrid network: A highly efficient and stable electrocatalyst for hydrogen evolution. Electrochem Commun 72:74–78
17. Zou ML, Zhang JF, Zhu H, Du ML, Wang QF, Zhang M, Zhang XW (2015) A 3D dendritic WSe2catalyst grown on carbon nanofiber mats for efficient hydrogen evolution. J Mater Chem A 3:12149–12153
18. Henckel DA, Lenz O, Cossairt BM (2017) Effect of Ligand Coverage on Hydrogen Evolution Catalyzed by Colloidal WSe2. ACS Catal 7:2815–2820
19. Wang XQ, Chen YF, Zheng BJ, Qi F, He JR, Li Q, Li PJ, Zhang WL (2017) Graphene-like WSe 2 nanosheets for efficient and stable hydrogen evolution. J Alloys Compd 691:698–704
20. Hussain S, Patil SA, Vikraman D, Arbab AA, Jeong SH, Kim HS, Jung J (2017) Growth of a WSe 2 /W counter electrode by sputtering and selenization annealing for high-efficiency dye-sensitized solar cells. Appl Surf Sci 406:84–90
21. Chen YX, Zhang WJ, Huang KJ, Zheng Ming B, Mao YC (2017) An electrochemical microRNA sensing platform based on tungsten diselenide nanosheets and competitive RNA–RNA hybridization. Analyst 142:4843–4851. https://doi.org/10.1039/c7an01244f
22. Wang X, Chen Y, Zheng B, Qi F, He J, Li Q, Zhang W (2017) Graphene-like $WSe_2$ nanosheets for efficient and stable hydrogen evolution. J Alloy Compd 691:698–704. https://doi.org/10.1016/j.jallcom.2016.08.305
23. Chen YX, Huang KJ, Lin F, Fang LX (2017) Ultrasensitive electrochemical sensing platform based on graphene wrapping $SnO_2$ nanocorals and autonomous cascade DNA duplication strategy. Talanta 175:168–176. https://doi.org/10.1016/j.talanta.2017.07.042
24. Radi AE, Acero Sánchez JL, Baldrich E, O'Sullivan CK (2005) Reusable impedimetric aptasensor. Anal Chem 77(19):6320–6323. https://doi.org/10.1021/ac0505775
25. Wang Y, Zhang Y, Yan T, Fan D, Du B, Ma H, Wei Q (2016) Ultrasensitive electrochemical aptasensor for the detection of thrombin based on dual signal amplification strategy of Au@GS and DNA-CoPd NPs conjugates. Biosens Bioelectron 80:640–646. https://doi.org/10.1016/j.bios.2016.02.042
26. Zheng Y, Yuan Y, Chai Y, Yuan R (2015) A label-free electrochemical aptasensor based on the catalysis of manganese porphyrins for detection of thrombin. Biosens Bioelectron 66:585–589. https://doi.org/10.1016/j.bios.2014.12.022
27. Yang J, Dou B, Yuan R, Xiang Y (2016) Proximity binding and metal ion-dependent DNAzyme cyclic amplification-integrated aptasensor for label-free and sensitive electrochemical detection of thrombin. Anal Chem 88(16):8218–8223. https://doi.org/10.1021/acs.analchem.6b02035
28. Umrao S, Jain V, Chakraborty B, Roy R (2018) Protein-induced fluorescence enhancement as aptamer sensing mechanism for thrombin detection. Sensors Actuators B Chem 267:294–301. https://doi.org/10.1016/j.snb.2018.04.039
29. Cao Y, Wang Z, Cao J, Mao X, Chen G, Zhao J (2017) A general protein aptasensing strategy based on untemplated nucleic acid elongation and the use of fluorescent copper nanoparticles: application to the detection of thrombin and the vascular endothelial growth factor. Microchim Acta 184:3697–3704. https://doi.org/10.1007/s00604-017-2393-y
30. He J, Li G, Hu Y (2017) Aptamer-involved fluorescence amplification strategy facilitated by directional enzymatic hydrolysis for bioassays based on a metal-organic framework platform: highly selective and sensitive determination of thrombin and oxytetracycline. Microchim Acta 184:2365–2373. https://doi.org/10.1007/s00604-017-2263-7